Article

Ligand K-Edge X-ray Absorption Spectroscopy of [FeS]$^{+}$ Clusters: Changes in Bonding and Electronic Relaxation upon Redox

Abhishek Dey, Thorsten Glaser, Manon M.-J. Couture, Lindsay D. Eltis, R. H. Holm, Britt Hedman, Keith O. Hodgson, and Edward I. Solomon

J. Am. Chem. Soc., **2004**, 126 (26), 8320-8328• DOI: 10.1021/ja0484956 • Publication Date (Web): 12 June 2004

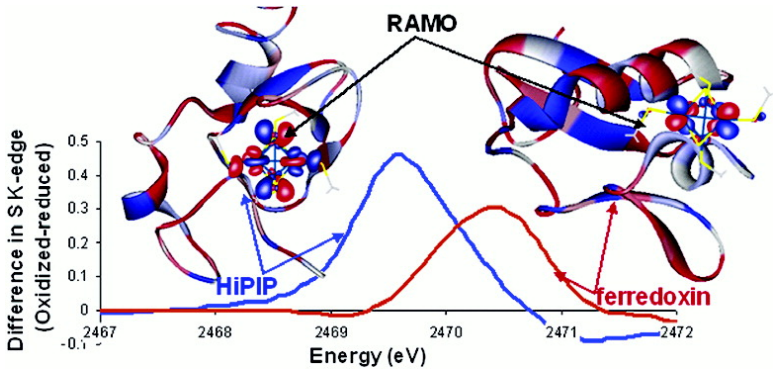

More About This Article

Additional resources and features associated with this article are available within the HTML version:

- Supporting Information
- Links to the 1 articles that cite this article, as of the time of this article download
- Access to high resolution figures
- Links to articles and content related to this article
- Copyright permission to reproduce figures and/or text from this article

View the Full Text HTML

Journal of the American Chemical Society is published by the American Chemical Society. 1155 Sixteenth Street N.W., Washington, DC 20036

J|A|C|S
ARTICLES
Published on Web 06/12/2004

Ligand K-Edge X-ray Absorption Spectroscopy of $[Fe_4S_4]^{1+,2+,3+}$ Clusters: Changes in Bonding and Electronic Relaxation upon Redox

Abhishek Dey,[†] Thorsten Glaser,[†,‡] Manon M.-J. Couture,[§] Lindsay D. Eltis,[⊥] R. H. Holm,[∥] Britt Hedman,*[,#] Keith O. Hodgson,*[,†,#] and Edward I. Solomon*[,†]

Contribution from the Department of Chemistry and Stanford Synchrotron Radiation Laboratory, Stanford University, Stanford, California 94305, Department of Microbiology and Biochemistry, University of British Columbia, Vancouver, Canada, V6T 1Z3, Department of Biochemistry, Université Laval, Quebec City, Canada, and Department of Chemistry and Chemical Biology, Harvard University, Cambridge, Massachusetts 02138

Received March 15, 2004; E-mail: edward.solomon@stanford.edu; hodgson@ssrl.slac.stanford.edu; hedman@ssrl.slac.stanford.edu

Abstract: Sulfur K-edge X-ray absorption spectroscopy (XAS) is reported for $[Fe_4S_4]^{1+,2+,3+}$ clusters. The results are quantitatively and qualitatively compared with DFT calculations. The change in covalency upon redox in both the $[Fe_4S_4]^{1+/2+}$ (ferredoxin) and the $[Fe_4S_4]^{2+/3+}$ (HiPIP) couple are much larger than that expected from just the change in number of 3d holes. Moreover, the change in the HiPIP couple is higher than that of the ferredoxin couple. These changes in electronic structure are analyzed using DFT calculations in terms of contributions from the nature of the redox active molecular orbital (RAMO) and electronic relaxation. The results indicate that the RAMO of HiPIP has 50% ligand character, and hence, the HiPIP redox couple involves limited electronic relaxation. Alternatively, the RAMO of the ferredoxin couple is metal-based, and the ferredoxin redox couple involves extensive electronic relaxation. The contributions of these RAMO differences to ET processes in the different proteins are discussed.

Introduction

Iron−sulfur proteins are ubiquitous in nature, performing many biological functions involving electron transfer and catalysis. The most common iron−sulfur proteins have mononuclear, binuclear, trinuclear, and tetranuclear clusters in their active site.[1,2] The four-iron clusters, found in bacterial ferredoxins and high potential proteins (HiPIPs), have four $\mu_3S_{sulfide}$, forming a cubane structure (Scheme 1), with one terminal $S_{cysteine}$ ligand for each Fe atom. These clusters generally perform one-electron transfer. The tetranuclear site undergoes two different biologically functional redox couples.[1a]

The HiPIP proteins cycle between the oxidized $[Fe_4S_4]^{3+}$ and the resting $[Fe_4S_4]^{2+}$ states (the HiPIP couple), whereas the bacterial ferredoxins cycle between the $[Fe_4S_4]^{2+}$ resting form and the reduced $[Fe_4S_4]^{1+}$ state (the ferredoxin couple). All three oxidation states have been isolated in proteins and inorganic model complexes.[2] The electronic structures of these states are well-known from detailed spectroscopic and computational studies.[3−7] The reduced $[Fe_4S_4]^{+}$ state has a valence-delocalized $[Fe_2S_2]^{+}$ subcluster antiferromagnetically coupled to an all-ferrous $[Fe_2S_2]^{0}$ subcluster. The spin states of these clusters are predominantly $S = 1/2$ in the protein active sites, while in the $[Fe_4S_4]^{+}$ model complexes higher spin states, $S = 3/2$ and $S = 5/2$ are also found.[8,17] The EPR silent resting form $[Fe_4S_4]^{2+}$

Scheme 1. Schematic Diagram of Fe_4S_4 Cluster in Bacterial Ferredoxin and HiPIP Proteins

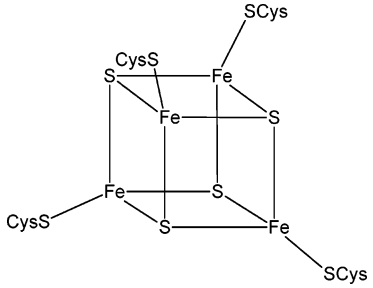

[†] Stanford University.
[‡] Present address: Institut für Anorganische und Analytische Chemie, Westfaelische Wilhelms-Universität Muenster, Germany.
[§] Université Laval.
[⊥] University of British Columbia.
[∥] Harvard University.
[#] Stanford Synchrotron Radiation Laboratory, SLAC, Menlo Park, CA, 94025.

(1) (a) *Iron-Sulfur Proteins*; Lovenberg, W., Ed.; Academic Press: New York, 1973−1977; Vols. I−III. (b) *Iron-Sulfur Proteins*; Spiro, T. G., Ed.; Metal Ions In Biology; Wiley-Interscience: New York, 1982; Vol. IV. (c) *Iron-Sulfur Proteins*; Cammack, R., Ed.; Advances in Inorganic Chemistry; Academic Press: San Diego, CA, 1992; Vol. 38. (d) *Iron-Sulfur Proteins*; Sykes, A. G., Cammack, R., Eds.; Advances in Inorganic Chemistry; Academic Press: San Diego, CA, 1999; Vol. 47. (e) Flint, D. D. H.; Allen, R. R. M. *Chem. Rev.* **1996**, *96*, 2315.
(2) Rao, P. V.; Holm, R. H. *Chem. Rev.* **2004**, *104*, 527.
(3) Beinert, H.; Holm, R. H.; Münck, E. *Science* **1997**, *277*, 653.
(4) Le Pape, L. L.; Lamotte, B. B.; Mouesca, J.-J. M.; Rius, G. *J. Am. Chem. Soc.* **1997**, *119*, 9757
(5) Czernuszewicz, R. S.; Macor, K. A.; Johnson, M. K.; Gewirth, A.; Spiro, T. G. *J. Am. Chem. Soc.* **1987**, *109*, 7178.
(6) Norman, J. G.; Ryan, P. B.; Noodleman, L. *J. Am. Chem. Soc.* **1980**, *102*, 4279.
(7) Noodleman, L.; Norman, J. G.; Osborne, J. H.; Aizman, A.; Case, D. A. *J. Am. Chem. Soc.* **1985**, *107*, 3418.

10.1021/ja0484956 CCC: $27.50

shows a characteristic Mössbauer spectrum, indicating that it has two valence-delocalized $[Fe_2S_2]^+$ subclusters antiferromagnetically coupled to give an $S = 0$ ground state.[3] The oxidized $[Fe_4S_4]^{3+}$ state has a valence-delocalized $[Fe_2S_2]^+$ subcluster antiferromagnetically coupled to an all-ferric $[Fe_2S_2]^{2+}$ cluster, resulting in a total spin state of $S = 1/2$.[4]

Ligand K-edge X-ray absorption spectroscopy (XAS) provides a direct estimate of ligand−metal bond covalencies.[9] The primary transition at the K-edge is the ligand 1s → 4p transition. However, because of the covalent mixing of the ligand 3p orbitals into the unoccupied metal 3d antibonding orbitals of Fe, transitions to these orbitals from the filled ligand 1s orbital obtain absorption intensity. This is derived from the electric-dipole allowedness of the intrinsic 1s → 3p transition. The intensity of this transition depends on the ligand character in the 3d antibonding orbital (α^2), from which the covalency of the metal−ligand bond can be quantified according to eq 1.

$$I(L_{1s} \rightarrow M_{3d}) = \alpha^2 I\langle L_{1s}|\boldsymbol{r}|L_{3p}\rangle \quad (1)$$

In eq 1, $I\langle L_{1s}|\boldsymbol{r}|L_{3p}\rangle$ is the transition moment integral or the intensity of a purely ligand 1s → 3p transition, which depends on the Z_{eff} of the ligand.[10] Thus, the pre-edge intensity provides a direct estimate of ligand−metal bond covalency.

A general methodology has been developed[11] for d^n systems where there can be multiple d^{n+1} final states. In these cases, the pre-edge intensity depends on the number of holes, the intensity redistribution into higher energy excited states due to CI, and the ligand−metal bond covalency. These factors have been considered in the analysis of ligand K-edge data of two series of complexes, $[MCl_4]^{2-}$ (M = Cu, Ni, Co, Fe, and Mn) and $[M(SR)_4]^{2-}$ (M = Ni, Co, Fe, and Mn).[11,12] A relation between ligand−metal bond covalency and the corrected (i.e., where these factors were taken into account) pre-edge intensity (D_o) has been derived from these analyses.

$$\alpha^2 = \frac{3D_o}{I\langle L_{1s}|\boldsymbol{r}|L_{3p}\rangle} \quad (2)$$

This method has previously been used to analyze the electronic structure and bonding of models and active sites of mononuclear Fe−S proteins (rubredoxins) and binuclear Fe_2S_2 proteins (spinach ferredoxin and Rieske protein).[13,14] The method has also been used to understand bonding in tetranuclear $[Fe_4S_4]^{2+}$ sites using model complexes having a single type of donor ligand, i.e., sulfide only in $[Fe_4S_4Cl_4]^{2-}$ or thiolate only in $[Fe_4Se_4(SPh)_4]^{2-}$.[15] In particular, the contribution of $\mu_3S_{sulfide}$ bridging to the electronic delocalization of the $[Fe_2S_2]^+$ subunit of a $[Fe_4S_4]^{2+}$ cluster was analyzed. In ref 15 it was shown that the decrease in bridging $\mu_3S_{sulfide}$ covalency in a $[Fe_4S_4]^{2+}$ cluster decreases the superexchange coupling, causing it to be delocalized because of double exchange.

In the present study, the S K-edge XAS of the model complex $[Fe_4S_4(SEt)_4]^{2-}$, having both thiolate and sulfide ligands, are analyzed and compared to results from DFT calculations on the resting $[Fe_4S_4]^{2+}$ site. The spectrum and the electronic structure of the resting state are then used as reference points to study the changes upon oxidation in the HiPIP couple and reduction in the ferredoxin couple. For the ferredoxin couple, model complexes of the reduced and resting state are studied, while for the HiPIP couple the study focuses on the enzyme active site to establish covalency changes with redox. For HiPIP, the protein and model data for the resting form are found to be very similar, indicating that the HiPIP centers are not significantly affected by the protein environment.

These S K-edge results are compared to DFT calculations for these couples to decompose the observed changes in electronic structure into contributions from the redox active molecular orbital (RAMO) and electronic relaxation. Electronic relaxation is the redistribution of charge density in a molecule upon oxidation to compensate for the hole produced and can make a significant contribution to ET processes. Recently, it has been shown, using a combination of variable energy photoelectron spectroscopy (VEPES) and DFT calculations, that in mononuclear iron tetrathiolate complexes the redox process involves extensive electronic relaxation, which contributes significantly to the thermodynamics and kinetics of ET in rubredoxin.[16] Here the possible contributions of the nature of the RAMO and electronic relaxation to the ET properties of the HiPIP and the ferredoxin redox couples will be considered.

Materials and Methods

Sample Preparation. The model complexes $[Bu_4N]_2[Fe_4S_4(SEt)_4]$ and $[Et_4N]_3[Fe_4S_4(SMe)_4]$ were prepared according to published methods.[17] For XAS experiments, sample preparations were performed in a dry, nitrogen-filled anaerobic atmosphere glovebox. The samples were ground into a fine powder and dispersed as thinly as possible on sulfur-free Mylar tape. This procedure has been verified to minimize self-absorption effects. The sample was then mounted across the window of an aluminum plate. A 6.35 μm polypropylene film window protected the solid samples from exposure to air during transfer from the glovebox to the experimental sample chamber.

The HiPIP protein was expressed from *Escherichia coli* as described in the literature.[18] The reduced protein solutions (in 100 mM phosphate buffer having pH 7.2−7.3) were pre-equilibrated in a water-saturated He atmosphere for ~1 h to minimize bubble formation in the sample cell. The protein sample was oxidized before experiments by using a ~3 to 4-fold excess of potassium ferricyanide. The solution was then loaded via a syringe into a Pt-plated Al block sample holder sealed in front using a 6.3 μm polypropylene window.

Data Collection and Reduction. XAS data were measured at the Stanford Synchrotron Radiation Laboratory using the 54-pole wiggler beam line 6-2. Details of the experimental configuration for low energy

(8) (a) Gloux, J. J.; Gloux, P. *J. Am. Chem. Soc.* **1995**, *117*, 7513. (b) Gloux, J. J.; Gloux, P. P.; Lamotte, B. B.; Mouesca, J.-J. M.; Rius, G. *J. Am. Chem. Soc.* **1994**, *116*, 1953.
(9) Glaser, T. G.; Hedman, B.; Hodgson, K. O.; Solomon, E. I. *Acc. Chem. Res.* **2000**, *33*, 859.
(10) Neese, F.; Hedman, B.; Hodgson, K. O.; Solomon, E. I. *Inorg. Chem.* **1999**, *38*, 4854.
(11) Shadle, S. E.; Hedman, B.; Hodgson, K. O.; Solomon, E. I. *J. Am. Chem. Soc.* **1995**, *117*, 2259.
(12) Rose Williams, K.; Hedman, B.; Hodgson, K. O.; Solomon, E. I. *Inorg. Chim. Acta* **1997**, *263*, 315.
(13) Rose, K.; Shadle, S. E.; Eidsness, M. K.; Kurtz, D. M., Jr.; Scott, R. A.; Hedman, B.; Hodgson, K. O.; Solomon, E. I. *J. Am. Chem. Soc.* **1998**, *120*, 10743.
(14) (a) Anxolabéhère-Mallart, E.; Glaser, T.; Frank, P.; Aliverti, A.; Zanetti, G.; Hedman, B.; Hodgson, K. O.; Solomon, E. I. *J. Am. Chem. Soc.* **2001**, *123*, 5444. (b) Rose, K.; Shadle, S. E.; Glaser, T.; de Vries, S.; Cherepanov, A.; Canters, G. W.; Hedman, B.; Hodgson, K. O.; Solomon, E. I. *J. Am. Chem. Soc*. **1999**, *121*, 2353
(15) Glaser, T.; Rose, K.; Shadle, S. E.; Hedman, B.; Hodgson, K. O.; Solomon, E. I. *J. Am. Chem. Soc.* **2001**, *123*, 442.
(16) Kennepohl, P.; Solomon, E. I. *Inorg. Chem.* **2003**, *42*, 679.
(17) Carney, M. J.; Papaefthymiou, G. C.; Spartalian, K.; Frankel, R. B.; Holm, R. H. *J. Am. Chem. Soc.* **1988**, *110*, 6084.
(18) Babini, E.; Borsari, M.; Capozzi, F.; Eltis, L. D.; Luchinat, C. *J. Biol. Inorg. Chem*. **1999**, *4*, 692.

studies have been described previously.[19] The energy calibration, data reduction, and error analysis follow the same methods described in ref 20.

Fitting Procedures. Pre-edge features were fit by pseudo-Voigt line shapes (sums of Lorentzian and Gaussian functions). This line shape is appropriate as the experimental features are expected to be a convolution of a Lorentzian transition envelope[21] and a Gaussian line shape imposed by the beam line optics.[22] A fixed 1:1 ratio of Lorentzian to Gaussian contribution successfully reproduced the pre-edge features. The rising edges were also fit with pseudo-Voigt line shapes. Fitting requirements included reproducing the data *and* its second derivative, using a minimum number of peaks. There are two components in the pre-edge region (sulfide and thiolate). Fits were performed using single peaks to simulate the pre-edge feature of each component with a half-width of 0.6 to 0.7 eV. Fits were also performed using two peaks for the sulfide to more accurately simulate the second derivative, which did not significantly change the total integrated areas and their mean energy positions. The energies of the pre-edge features of the reduced model complex and protein were allowed to vary by 0.1 to 0.2 eV from the values obtained from previous studies (2470.1 eV for $Fe^{2.5}-\mu_3S_{sulfide}$[15] and 2470.9 eV for $Fe^{2.5}-S_{thiolate}$[13]), to allow for shifts due to oxidation or reduction of the Fe centers. The intensity of a pre-edge feature (peak area) represents the sum of the intensity of all the pseudo-Voigt peaks which were needed to successfully fit the feature in a given fit. The reported intensity values for both the model complexes and the proteins are an average of all of the accepted pre-edge fits, typically 6−8 (which differed from each other by less than 3%).

DFT Calculations. All calculations were performed on IBM 3BT-RS/6000 work stations and a SGI Origin 2000 computer using the Amsterdam density functional (ADF) program, versions 2002.03 and ADF 2000, developed by Baerends et al.[23,24] A triple-ζ Slater-type orbital basis set (ADF basis set TZP) with a single polarization function at the local density approximation of Vosko, Wilk, and Nusair[25] with nonlocal gradient corrections of Becke[26] and Perdew[27] were employed. The crystal structure of the model complex $[Fe_4S_4(SEt)_4]^{2-}$ was optimized to C_2 symmetry and used for all calculations (See table S1 in the Supporting Information). The electronic structures of the clusters were calculated in the spin unrestricted broken symmetry state.[28] The density of states (DOS) is a sum of pseudo-Voigt curves having amplitudes given by the calculated orbital covalencies, centered at the respective orbital energy (see Supporting Information for more details) and with a peak width given by that of a single pre-edge transition (0.45 eV). On the basis of previous results, an offset of 0.8 eV was applied to the thiolate DOS relative to the sulfide DOS to account for difference between the 1s orbital energies.

Results

S K-Edge XAS of $[Fe_4S_4(SEt)_4]^{2-}$. The S K-edge of the resting form $[Fe_4S_4(SEt)_4]^{2-}$ model complex (Figure 1a) shows two distinct features. There is a broad, intense pre-edge feature, between 2469 and 2472 eV, involving transitions from the ligand 1s orbitals to the metal antibonding orbitals, and another intense rising edge feature, at 2473.0 eV, corresponding to the thiolate 1s → C−S σ* transitions.[12] The pre-edge feature represents an

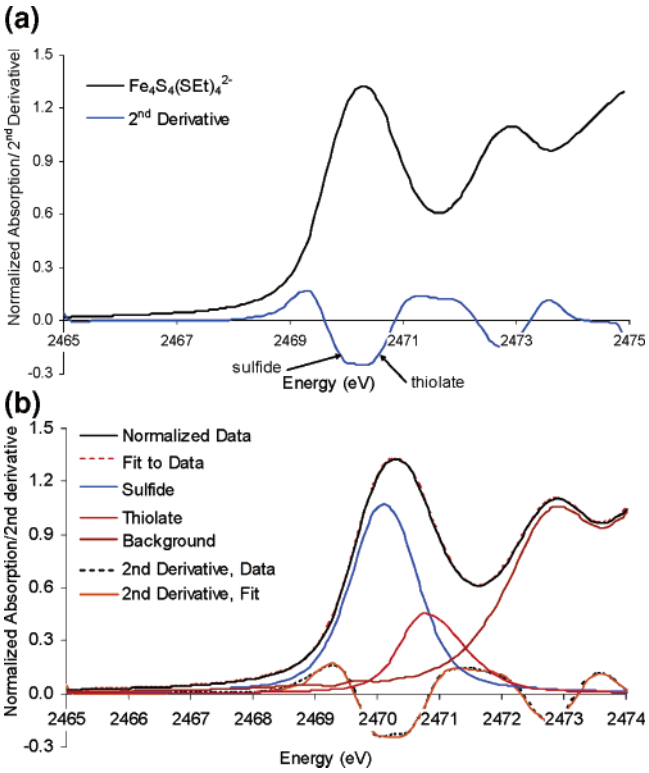

Figure 1. (a) S K-edge XAS spectrum of the model complex $[Fe_4S_4(SEt)_4]^{2-}$ and the second derivative showing sulfide and thiolate contributions. (b) S K-edge XAS spectrum of the model complex $[Fe_4S_4(SEt)_4]^{2-}$, the fitted data, the fit components from sulfide and thiolate transitions, and the second derivative data and its fit.

envelope of transitions from both $\mu_3S_{sulfide}$ and $S_{thiolate}$ 1s orbitals to the d-antibonding manifold. It has been previously determined, using sulfide-only and thiolate-only model complexes, that the pre-edge transitions from the $\mu_3S_{sulfide}$ 1s orbital are at ∼2470.2 eV, 0.8 eV lower in energy than the transitions from the 1s orbital of $S_{thiolate}$ (at ∼2471.0 eV).[15] Fits to the experimental spectrum and its second derivative (Figure 1b) give the relative contributions of the $\mu_3S_{sulfide}$- and $S_{thiolate}$-based transitions to the pre-edge intensity (D_o in Table 1). This pre-edge intensity is related to the total percentage ligand character in the d antibonding manifold by eq 2. The transition moment integrals ($\langle L_{1s}|\boldsymbol{r}|L_{3p}\rangle$) for specific ligands have been determined by relating the pre-edge intensities of model complexes whose percentage ligand character in the d antibonding manifold is known from independent experiments.[9] Note that the thiolate ligand has a higher transition moment integral (namely, $I\langle L_{1s}|\boldsymbol{r}|L_{3p}\rangle = 8.05$ for thiolate and 6.54 for sulfide), and hence, the thiolate pre-edge feature is more intense than that of the sulfide for the same percentage ligand character in the accepting orbital. As a result, the relative pre-edge intensities (D_o) do not directly reflect the relative bond covalencies of these ligands (Figure 1b). The experimental D_o value gives the total ligand character summed up over 18 holes, present in the resting form, using eq 2. A D_o of 1.72 for sulfide in $[Fe_4S_4(SEt)_4]^{2-}$ gives a total hole sulfide character of 492%, and a D_o of 0.70 for thiolate gives a total hole thiolate character of 164%. This total intensity is then divided by the number of ligand−metal bonds present in the complex (12 $\mu_3S_{sulfide}$−Fe bonds and four $S_{thiolate}$−Fe bonds) to get an average ligand−metal bond covalency. The

(19) Hedman, B.; Frank, P.; Gheller, S. F.; Roe, A. L.; Newton, W. E.; Hodgson, K. O. *J. Am. Chem. Soc.* **1988**, *110*, 3798.
(20) Shadle, S. E.; Hedman, B.; Hodgson, K. O.; Solomon, E. I. *Inorg. Chem.* **1994**, *33*, 4235.
(21) Agarwal, B. K. *X-ray Spectroscopy*; Springer-Verlag: Berlin, 1979; pp 276 ff.
(22) Tyson, T. A.; Roe, A. L.; Frank, P.; Hodgson, K. O.; Hedman, B. *Phys. Rev. B* **1989**, *39A*, 6305.
(23) Baerends, E. J.; Ellis, D. E.; Ros, P. *Chem. Phys.* **1973**, *2*, 41.
(24) te Velde, G.; Baerends, E. J. *Int. J. Comput. Phys.* **1992**, *99*, 84.
(25) Vosko, S. H.; Wilk, L.; Nusair, M. *Can. J. Phys.* **1980**, *58*, 1200.
(26) Becke, A. D. *J. Chem. Phys.* **1986**, *84*, 4524.
(27) Perdew, J. P. *Phys. Rev. B* **1986**, *33*, 8822.
(28) Noodleman, L. *J. Chem. Phys.* **1981**, *74*, 5737.

Table 1. S K-Edge XAS Results of $[Fe_4S_4]$ Model Complexes and Proteins

	sulfide			thiolate		
	D_0	energy (eV)	covalency per Fe–S bond (%)[a]	D_0	energy (eV)	covalency per Fe–S bond (%)[a]
$[Fe_4S_4(SEt)_4]^{2-}$	1.72 ± 0.05	2470.1 ± 0.1	41 ± 1	0.70 ± 0.04	2470.9 ± 0.1	41 ± 1
$[Fe_4S_4(SMe)_4]^{3-}$	1.59 ± 0.08	2470.2 ± 0.1	38 ± 2	0.59 ± 0.1	2471.1 ± 0.1	34 ± 2
$[Fe_4S_4(SCys)_4]^{2-}$ HiPIP resting	1.55 ± 0.05	2470.1 ± 0.1	37 ± 1	0.69 ± 0.06	2470.9 ± 0.1	40 ± 2
$[Fe_4S_4(SCys)_4]^{-}$ HiPIP oxidized	1.83 ± 0.03	2470.0 ± 0.1	44 ± 1	0.81 ± 0.06	2470.8 ± 0.1	48 ± 2

[a] Obtained by using eq 2 and dividing the total hole covalency by the number of bonds: 12 for sulfide and four for thiolate.

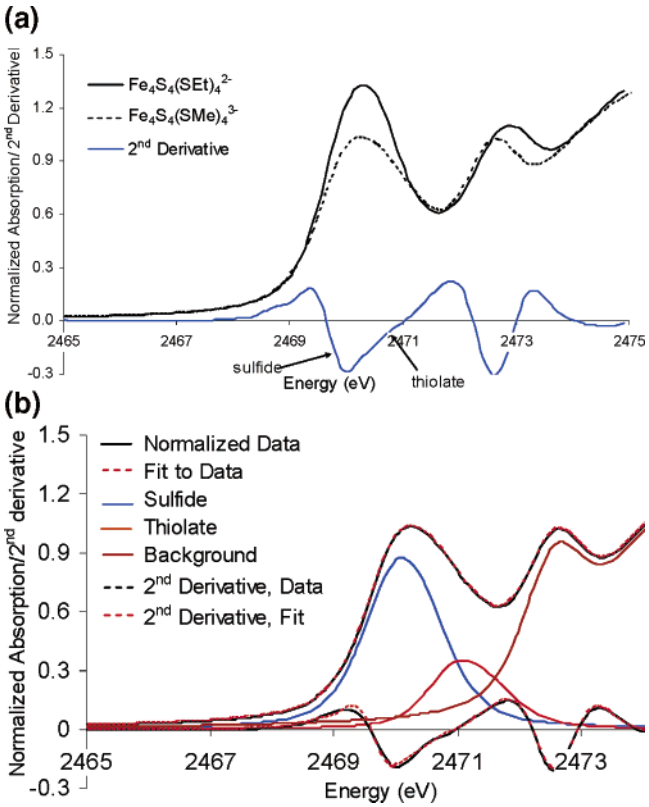

Figure 2. (a) S K-edge XAS spectrum of $[Fe_4S_4(SEt)_4]^{2-}$ and $[Fe_4S_4(SMe)_4]^{3-}$ and the second derivative of $[Fe_4S_4(SMe)_4]^{3-}$ showing the components. (See Figure S2 in the Supporting Information for an expanded energy region plot.) (b) S K-edge XAS spectrum of the model complex $[Fe_4S_4(SMe)_4]^{3-}$, the fitted data, the fit components from sulfide and thiolate transitions, and the second derivative data and its fit.

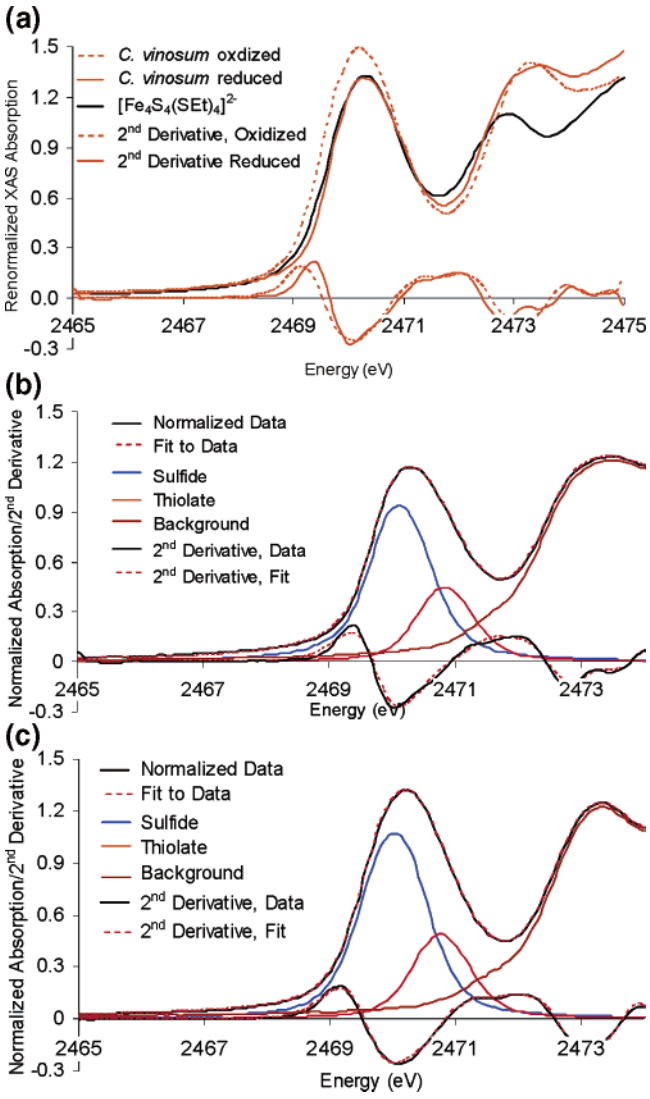

Figure 3. (a) S K-edge XAS spectrum of the model complex $[Fe_4S_4(SEt)_4]^{2-}$ and S K-edge XAS and second derivative of the experimental spectrum of HiPiP protein in its resting $[Fe_4S_4]^{2+}$ form and in its oxidized form. (See Figure S1 in the Supporting Information for an expanded energy region plot.) (b) S K-edge XAS spectrum of resting form of HiPIP, the fitted data, the fit components from sulfide and thiolate transitions, and the second derivative data and its fit. (c) S K-edge XAS spectrum of oxidized form of HiPiP, the fitted data, the fit components from sulfide and thiolate transitions, and the second derivative data and its fit.

average covalencies of Fe−μ_3S$_{sulfide}$ and Fe−S$_{thiolate}$ bonds are both found to be 41% (Table 1).[29]

S K-Edge XAS of $[Fe_4S_4(SMe)_4]^{3-}$. The S K-edge spectrum of the reduced model complex, $[Fe_4S_4(SMe)_4]^{3-}$, (Figure 3a) shows two distinct broad features similar to the spectrum of the resting-form $[Fe_4S_4(SEt)_4]^{2-}$ model complex. The pre-edge between 2469.0 and 2472.0 eV involves transitions from the ligand 1s to the metal d-antibonding orbitals. The transition at 2472.5 eV is the thiolate 1s to C−S σ^* transition. The second derivative to the experimental spectrum (blue line in Figure 2a) shows the presence of distinct contributions to the pre-edge from μ_3S$_{sulfide}$ and S$_{thiolate}$. The fits to the experimental spectrum and its second derivative (Figure 2b) give μ_3S$_{sulfide}$ and S$_{thiolate}$ contributions to the pre-edge intensities (D_0) as 1.59 and 0.59, respectively. These correspond to average Fe−μ_3S$_{sulfide}$ and Fe−S$_{thiolate}$ bond covalencies of 38% and 34%, respectively (Table 1). The intensity of the pre-edge has decreased significantly, and it appears to be broader than the pre-edge of $[Fe_4S_4(SEt)_4]^{2-}$. Since the ligand environment in the reduced model complex is very similar to that of the resting state model complex (there is negligible difference between donor properties of SMe and SEt), the decrease of pre-edge intensity is in part attributed to loss of

(29) Note that the numbers here differ slightly from published values in ref 31 as the contributions of sulfide and thiolate to the pre-edge intensity was fit separately rather than using reference spectra. The differences are all less than 2%.

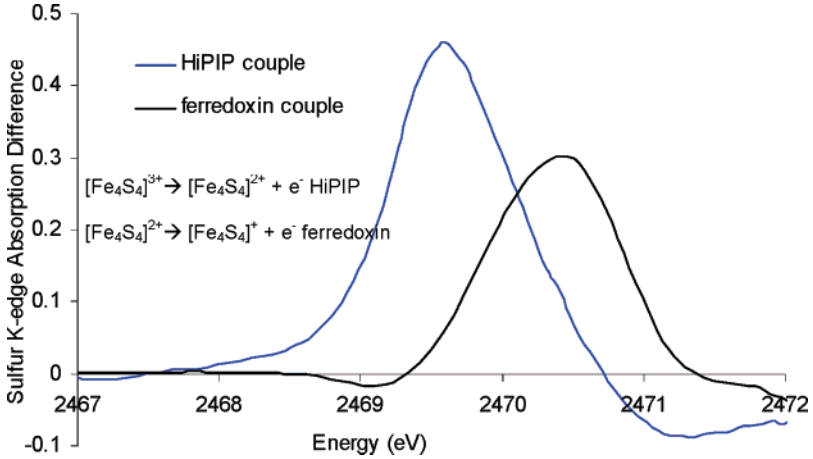

Figure 4. Difference of S K-edge XAS of HiPIP and ferredoxin couple. The difference spectra were calculated by subtracting the resting form spectrum from the corresponding oxidized protein and by subtracting the reduced model spectrum from the resting model spectrum.

one hole in the reduced model complex relative to the resting form. An estimate of this contribution to the intensity decrease can be made based on average covalency per hole of the resting state $[Fe_4S_4(SEt)_4]^{2-}$ complex. Subtracting this average ligand character of one hole from the total hole covalency of the resting form gives an estimate of the covalencies of the reduced cluster as 39% for both the Fe−$\mu_3S_{sulfide}$ and the Fe−$S_{thiolate}$ bonds. However, the actual bond covalencies are less than this (38 and 34%, respectively). Thus, the decrease in pre-edge intensity is more than that expected from a decrease by one hole and provides insight into the nature of the RAMO and the presence of electronic relaxation in the redox process involving the $[Fe_4S_4]^{2+/+}$ couple. Note that the sulfide and thiolate pre-edge transitions shift to a higher energy in the reduced model complex compared to those of the resting-form $[Fe_4S_4(SEt)_4]^{2-}$ complex. The sulfide feature shifts by 0.1 eV (Table 1, from 2470.1 to 2470.2 eV) while the thiolate pre-edge feature shifts by 0.2 eV (Table 1, from 2470.9 to 2471.1 eV). This is due to the decreased Z_{eff} on the Fe with reduction, which shifts the d-manifold to higher energy. Also note that the C−S σ^* transitions shift from 2472.2 to 2472.7 eV from the reduced to the resting-form model complex. This is due to a combination of lower 1s orbital energy of the $S_{thiolate}$ and stronger C−S bonding (raising C−S σ^* orbital energy) in the resting-form model complex.

S K-Edge of Resting HiPIP Protein. The S K-edge XAS spectrum of the active site of the HiPIP protein (Figure 3a) from *Chromatium vinosum*, in its resting form, is very similar to that of the resting-form model complex $[Fe_4S_4(SEt)_4]^{2-}$ (black line in Figure 3a). Fits to the experimental data (Figure 3b) give $\mu_3S_{sulfide}$ and $S_{thiolate}$ pre-edge intensities of 1.55 and 0.69, respectively. These correspond to average covalencies of 37 and 40% for the Fe−$\mu_3S_{sulfide}$ and Fe−$S_{thiolate}$ bonds, respectively (Table 1).[30] The slight decrease in the covalencies of the protein active site compared to the model (4% for Fe−$\mu_3S_{sulfide}$ and 1% for Fe−$S_{thiolate}$) is due to the presence of H-bonding in the protein active site.[31] Note that this difference in covalency is higher for the $\mu_3S_{sulfide}$ as these have higher electron density and are more affected by H-bonds.

(30) Note that the numbers here are ∼3−5% higher than results published in ref 31 because of higher purity of the protein sample (see ref 32).
(31) Glaser, T.; Bertini, I.; Moura, J. J. G.; Hedman, B.; Hodgson, K. O.; Solomon, E. I. *J. Am. Chem. Soc.* **2001**, *123*, 4859.

S K-Edge of Oxidized HiPIP Protein. The S K-edge XAS spectrum of the oxidized HiPIP protein (Figure 3a) also shows the two broad and intense bands characteristic of Fe_4S_4 clusters. The pre-edge is centered around 2468.5−2471 eV, and the rising edge transition is centered at around 2473 eV. Fits to the experimental spectrum and its second derivative (Figure 3c) give the contributions of $\mu_3S_{sulfide}$ and $S_{thiolate}$ to the pre-edge intensity (D_o) as 1.80 and 0.81, respectively. These give average Fe−$\mu_3S_{sulfide}$ and Fe−$S_{thiolate}$ bond covalencies of 44 and 48%, respectively. Hence, there is an increase in pre-edge intensity in the oxidized relative to the resting protein site. An increase in pre-edge intensity on oxidation is expected as the number of acceptor holes has increased to 19, from 18 in the resting state. An estimate of this contribution to the increase in pre-edge intensity can be made by adding the average one-hole covalency of the resting form of the HiPIP protein to its total hole covalency. This gives 39 and 42% for Fe−$\mu_3S_{sulfide}$ and Fe−$S_{thiolate}$, respectively, as the covalencies of the oxidized cluster. This increase of 7 and 8% in the observed Fe−$\mu_3S_{sulfide}$ and Fe−$S_{thiolate}$ covalencies provides insight into the RAMO involved and nature of the electronic relaxation in the redox process and will be addressed in the following sections. The pre-edge position of the oxidized protein shifts down by 0.1 eV relative to that of the resting site. The shift in the pre-edge energy position reflects the increase in Z_{eff} of the iron atoms upon oxidation, which shifts the d-manifold acceptor orbitals to lower energy. Also note that there is a shift of the thiolate 1s → C−S σ^* position from 2472.8 eV in the resting form to 2473.2 eV in the oxidized form. The shift is not clear in the experimental spectra of the protein (Figure 3a) because of the broad nature of the peaks. However, the shift is clearly visible in the second derivative of the spectra where the first minimum after the pre-edge region indicates the position of this transition. This is due to lower energy of the 1s orbital of the $S_{thiolate}$ and the stronger C−S bonding (shifting the C−S σ^* orbital to higher energy) upon oxidation.

Differential Changes on Redox in HiPIP and Ferredoxin Couples. In both the HiPIP and the ferredoxin redox couples (Figure 4), the changes in metal−ligand bond covalency are more than that expected on the basis of ground state hole covalencies. Additionally, the difference between the S K-edge XAS spectrum of the oxidized and the reduced partners (Figure

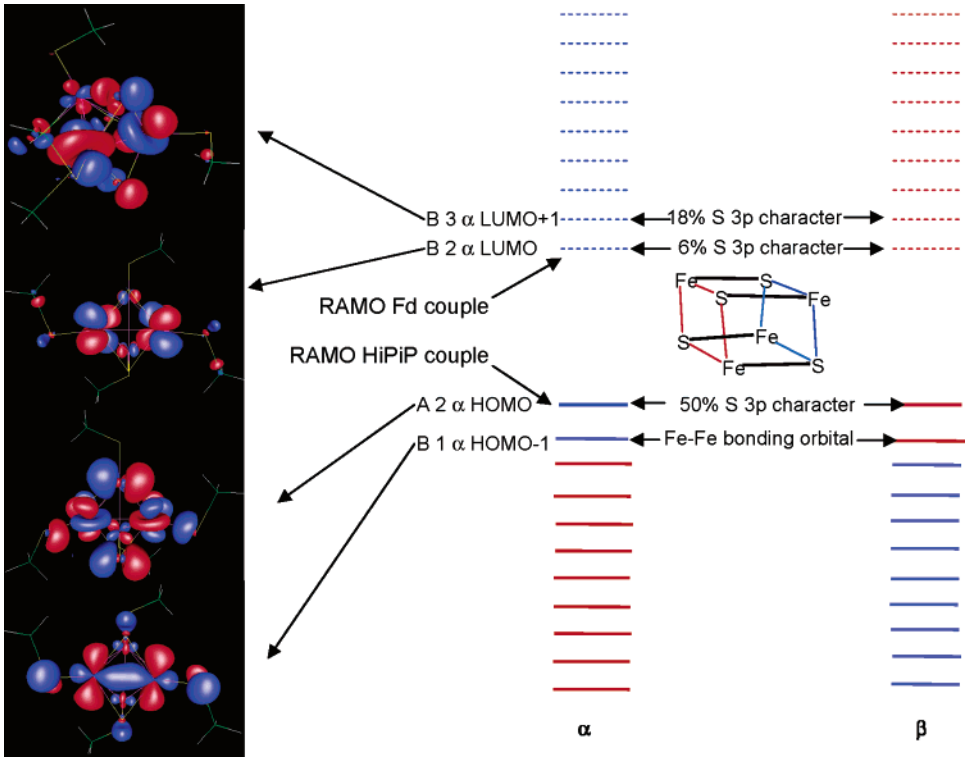

Figure 5. Schematic molecular orbital diagram of the cluster in the resting $[Fe_4S_4]^{2+}$ form. The two delocalized $[Fe_2S_2]^{+}$ subclusters A and B are colored blue and red. The occupied orbitals are represented by bold lines while the unoccupied orbitals are represented by dotted lines. The cluster is C_2 symmetric, and hence only the α orbitals are described below. All the orbitals delocalized over subclusters A and B are labeled accordingly. The HOMO − 1 (B1) is $d_{x^2-y^2} + d_{x^2-y^2}$ bonding orbital, the HOMO (A2) is $d_{x^2-y^2} - d_{x^2-y^2}$ antibonding orbital with 50% ligand character, and the LUMO (B2) is an Fe−Fe antibonding orbital with 6% ligand character.

4) shows that the change in intensity in the HiPIP couple is more than that in the Fd couple. This difference is quantified by the fits to the spectra (Table 1). The total ligand character ($12 \times$ Fe$-\mu_3$S$_{sulfide}$ covalency $+ 4 \times$ Fe$-$S$_{thiolate}$ covalency) changes by 107% for the HiPIP couple as compared to only 66% for the ferredoxin couple. Since both processes involve creation of one hole, the observed difference between these couples is important.

Analysis

DFT Calculations on the Resting $[Fe_4S_4]^{2+}$ State. DFT calculations were performed on the resting form of the cluster to quantitatively compare to the ligand K-edge results. These will then be used to evaluate the relative contributions of the nature of RAMO and electronic relaxation to the change in metal−ligand bond covalency observed experimentally upon reduction/oxidation.

The ground-state wave function obtained for the resting $[Fe_4S_4]^{2+}$ form gives two $S = 9/2$ delocalized $[Fe_2S_2]^{+}$ subclusters, antiferromagnetically coupled to give an $S = 0$ ground state, a result well-known from spectroscopic and computational studies.[3,6] A schematic molecular orbital diagram, obtained from the calculations, is given in Figure 5. Each $S = 9/2$ delocalized $[Fe_2S_2]^{+}$ subcluster (in blue and in red) has 10 occupied α (or β) spin−orbitals (in bold), one occupied β (α) spin−orbital, and nine unoccupied orbitals (dotted lines) delocalized over the two iron atoms. Since the cluster has C_2 symmetry, only the relevant α orbitals are described, which are also labeled by the subcluster on which they are localized (A or B). The HOMO (A2α in Figure 5) is the $d_{x^2-y^2} - d_{x^2-y^2}$ antibonding orbital having 50% ligand character. The minority spin bonding $d_{x^2-y^2} + d_{x^2-y^2}$ orbital (B1α in Figure 5) from subcluster B, which is believed to be the HOMO in a delocalized reduced two-iron ferredoxin $[Fe_2S_2]^{+}$ cluster, is the HOMO − 1 in this case. This is due to strong Fe−Fe interaction in the $[Fe_4S_4]$ clusters,[32,33] which stabilizes this minority spin Fe−Fe bonding orbital of the $[Fe_2S_2]^{+}$ unit of the cluster. The LUMO (B2α in Figure 5) is an Fe−Fe antibonding orbital having 6% ligand character.

The calculated covalencies (percent individual ligand characters summed over all metal 3d holes) are 25 and 28% for Fe$-\mu_3$S$_{sulfide}$ and Fe$-$S$_{thiolate}$ bonds, respectively, which are quantitatively about 16 and 13%, respectively, less than the experimentally obtained bond covalencies (from Table 1). The calculated per hole covalencies are about 2% less than experiment. The above DFT calculations used a pure density functional (BP86) which is usually found to overestimate the covalency with respect to experiment. It is therefore important to first evaluate the process of obtaining numerical estimates of bond covalencies from pre-edge intensities.

The experimentally obtained metal−ligand bond covalencies could have errors due to: (a) inaccurate transition moment integral (D_o) and (b) an error in distributing intensities between sulfide and thiolate as these have different D_o values. The transition moment integrals used here are those of the S−Cys bond in plastocyanin[34] for thiolate and μ_2S$_{sulfide}$ in CsFeS$_2$[14a] for μ_3S$_{sulfide}$, which were obtained by correlating pre-edge intensities of these complexes to known values of total hole

(32) Noodleman, L.; Norman, J. G.; Osborne, J. H.; Aizman, A.; Case, D. A. *J. Am. Chem. Soc.* **1985**, *107*, 3418.
(33) Mouesca, J. M.; Chen, J. L.; Noodleman, L.; Bashford, D.; Case, D. A. *J. Am. Chem. Soc.* **1994**, *116*, 11898.
(34) Shadle, S. E.; Penner-Hahn, J. E.; Schugar, H. J.; Hedman, B.; Hodgson, K. O.; Solomon, E. I. *J. Am. Chem. Soc.* **1993**, *115*, 767.

Table 2. Correlation between Theoretically Estimated and Experimentally Observed Changes in Total Covalency of Different Redox Couples

	system		total hole covalency[a] sulfide (%)	total hole covalency[a] thiolate (%)	No. of holes	ligand character per hole (%)[b]	change in total ligand character on redox (%)[c]
Fd couple	$[Fe_4S_4](SEt)_4^{2-}$ model expt		41	41	18	36.5	−10.2
	$[Fe_4S_4](SMe)_4^{3-}$ model expt		38	34	17	34.7	
HiPIP couple	$[Fe_4S_4](SCys)_4^{2-}$ protein expt		37	40	18	34.2	+16.0
	$[Fe_4S_4](SCys)_4^{1-}$ protein expt		44	48	19	37.6	
resting	$[Fe_4S_4](SMe)_4^{2-}$ theory		25	28	18	23	
reduced	$[Fe_4S_4](SMe)_4^{3-}$ theory unrelaxed	1/2	25	27	17	23.9	−1.9
		3/2	27	30	17	26.5	+8.7
	$[Fe_4S_4](SMe)_4^{3-}$ theory relaxed	1/2	23	19	17	20.2	−10.1
		3/2	24	20	17	21.9	−16.9
oxidized	$[Fe_4S_4](SMe)_4^{1-}$ theory unrelaxed		29	31	19	24.8	+13.8
	$[Fe_4S_4](SMe)_4^{1-}$ theory relaxed		30	35	19	26.4	+21.0

[a] Experimental total hole covalency is derived from the intensity of transitions to the empty Fe_{3d} antibonding orbitals from 1s orbitals of both types of ligands. [b] Observed or calculated total covalency over all holes divided by number of holes. [c] Decrease in covalency is indicated by a negative sign and increase by a positive sign.

covalencies obtained from independent experiments. The transition moment integral is a function of the Z_{eff} of the ligand atom.[10] However, the Z_{eff} is not expected to change significantly in the ligands considered here ($S_{thiolate}$ and $\mu_3S_{sulfide}$) relative to their respective calibrants.[35] Hence, the transition moment integrals used above are reasonable. The second factor which could effect the estimation of covalency from pre-edge intensities is the incorrect distribution of the pre-edge intensity between the two donors. This can also be ruled out because similar differences between the DFT-calculated covalency and S K-edge results have been observed in cases with only one type of sulfur donor. In particular, the covalency of Fe−$\mu_3S_{sulfide}$ bond obtained from the pre-edge intensity of $[Fe_4S_4Cl_4]^{2-}$ is 39%, whereas the calculated covalency is 24%, and the covalency of Fe−$S_{thiolate}$ bond obtained from the pre-edge intensity of $[Fe_4Se_4(SPh)_4]^{2-}$ is 38%, whereas the calculated covalency is 26%.[36]

Thus, these results indicate that DFT at the GGA level underestimates the increased bonding in these clusters. Alternatively, the DFT calculations give a good description of relative bonding interactions of the different ligands in these clusters. A DOS is constructed by plotting the calculated orbital covalencies against orbital energy for $\mu_3S_{sulfide}$ and $S_{thiolate}$ (Figure 6). An offset of 0.8 eV is used for thiolate to account for the difference in its 1s orbital energy relative to the $\mu_3S_{sulfide}$.[15] This DOS is then used to theoretically predict the pre-edge region of the S K-edge XAS of $[Fe_4S_4(SEt)_4]^{2-}$. This requires a scaling to take into account the different transition moment integrals of thiolate and $\mu_3S_{sulfide}$. The result is in good agreement with the experimental pre-edge data. This suggests that although the bonding description obtained from DFT calculations at the GGA level are quantitatively too ionic for the Fe_4S_4 system, the relative bonding interactions of sulfide and thiolate are well-described.

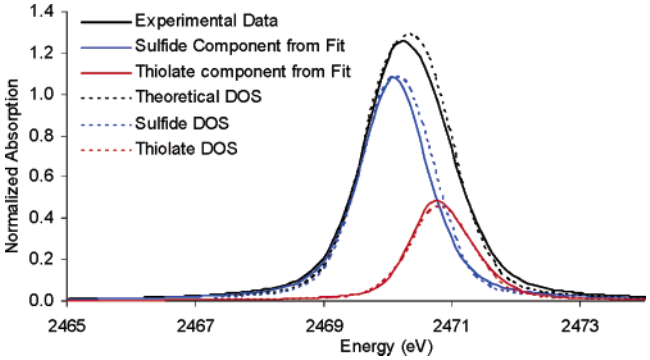

Figure 6. Experimental data and fit pre-edge components and calculated DOS for total pre-edge and components sulfide and thiolate. (See Figures S4 and S5 for details on DOS of sulfide and thiolate.)

RAMO and Electronic Relaxation Effects on the $[Fe_4S_4]^{3+/2+}$ and $[Fe_4S_4]^{2+/+}$ Redox Couples. In the following sections, the observed changes in the S K-edge XAS on oxidation will be decomposed into contributions from the nature of the RAMO and from electronic relaxation, and a model for differences in the redox processes in HiPIP and ferredoxins will be developed. Since these clusters show only small changes in geometry between different redox states, geometric relaxation has a small effect and is not considered in the following analysis.

HiPIP Couple. The changes in pre-edge intensity on oxidation of the HiPIP active site (Figure 3c and Table 1) are larger than that expected from a simple increase of one hole, assuming the covalency of this hole is equal to the average covalency of

(35) Note that the I_o has to increase by 33% for the experimentally observed metal−ligand covalency to be comparable to the calculated covalency. An increase in I_o will require an increase in Z_{eff} relative to the Z_{eff} of the calibrant. Z_{eff} will increase with increase in covalency. Therefore, an increase in I_o to reduce experimental estimates of covalency will require an increase in covalency, which means increasing intensity.

(36) The model complex $[Fe^{III}(S_2\text{-}o\text{-}xyl)_2]^-$ has been well-characterized using photoelectron spectroscopy (PES), and the covalency of the Fe−$S_{thiolate}$ bond in this complex is known to be 45%. The Fe−$S_{thiolate}$ bond covalency obtained from pre-edge intensity of the S K-edge XAS spectrum of this complex is 43%, very close to the value obtained by PES. However, both single-point and geometry-optimized DFT calculations (at a GGA level) on this complex indicate that the Fe−$S_{thiolate}$ bond covalency is 29 to 30%. This parallels the difference between the calculated and experimental metal−ligand bond covalencies observed here.

the holes of the resting $[Fe_4S_4]^{2+}$ state. DFT calculations on the resting form show that the RAMO for the HiPIP couple (HOMO, A2α in Figure 5) has more than 50% ligand character.[37] An estimate of the increase of the total ligand character due to removal of an electron from the RAMO (without relaxation, Table 2) shows that the total ligand character (summed over all holes) should increase by 13.8% (Table 2) of the total ligand character in the resting state. The experimentally observed increase for the HiPIP protein is 16% of the total hole covalency of the resting form, which is close to the unrelaxed estimate. On allowing the electronic structure to relax, the increase in total ligand character is about 21% (relaxed, Table 2) higher than the experimental result, though still reasonable. Hence, for the HiPIP couple only one third of the total calculated increase in the ligand character on oxidation (7% of 21%) is from electronic relaxation. Thus, most of the increase in ligand character is derived from the RAMO involved in the HiPIP couple in Figure 5 (A2α HOMO). The deviation of the calculated total change (+21%) from the experimentally observed total change (+16%) may be due to difference in the geometry of the model complex $[Fe_4S_4(SEt)_4]^{2-}$, on which the calculation has been performed, and protein active site contributions.

Ferredoxin Couple. The ligand S K-edge XAS of the ferredoxin couple (investigated here using the model complexes) also shows a larger decrease in ligand character upon reduction than expected based on the average covalency of the resting state. The total ligand character changes by −10.2% relative to the resting form, upon reduction, in the ferredoxin couple. Note that though the reduced protein sites have $S = 1/2$ ground states, the reduced model complex $[Fe_4S_4(SMe)_4]^{3-}$ is a physical mixture of $S = 1/2$ and $S = 3/2$ states.[8] Thus, we need to consider a mean of the changes calculated for these two different reduced states in the analysis. The $S = 1/2$ state can be achieved by adding an electron to the LUMO (B2α in Figure 5) of the resting $[Fe_4S_4]^{2+}$ form, which has only 6% ligand character. This reduces the total hole covalency by −1.9% (reduced, theory unrelaxed, $S = 1/2$, Table 2). The $S = 3/2$ state is achieved by a spin-forbidden transition creating a hole in the HOMO (A2α in Figure 5, 50% S character) and occupying the LUMO + 1 (B3 α in Figure 5, 18% S character) upon reduction of the LUMO. This increases the total covalency by 8.9% (reduced, theory unrelaxed, $S = 3/2$, Table 2). The mean of these changes indicates that on reduction the covalency of the model complex should increase by 3.5% when experimentally it is observed to decrease by −10.2%.

After allowing for electronic relaxation in these calculations (reduced, theory relaxed, Table 2), the ligand character changes by −16.9 and −10.1% for $S = 1/2$ and $S = 3/2$ states, respectively. Now, the mean of these changes show that on reduction the covalency should decrease by −13.5%, which is close to the experimental results. Thus, electronic relaxation is needed to account for the observed decrease in total ligand character in the ferredoxin couple.

In summary, in the ferredoxin couple (involving the $S = 1/2$ reduced state) the RAMO is a metal-based orbital (B2α in Figure 5, 6% ligand character) and adding an electron to this orbital will induce extensive electronic relaxation, which in the HiPIP couple, the RAMO is rich in ligand character and electronic relaxation effects are small.

(37) Similar results were obtained by Xα calculations by Noodleman and coworkers in ref 33.

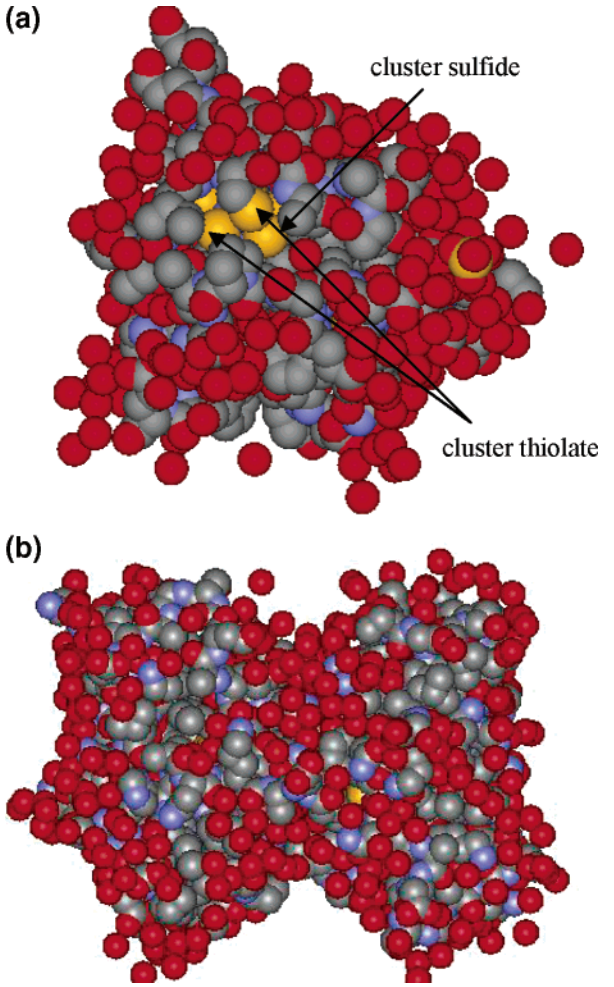

Figure 7. (a) A spacefill model of the ferredoxin protein from *Bacillus thermoproteolyticus*.[40] The cluster sulfide and thiolate sulfurs are visible from the surface, indicating that the cluster is solvent-exposed. (b) A spacefill model of HiPIP protein from *C. vinosum*[39] obtained from the crystal structure of protein. Note that the cluster is not visible from the surface.

Discussion

Electronic Relaxation in HiPIPs and Ferredoxins. The schematic MO diagram of the resting $[Fe_4S_4]^{2+}$ form in Figure 5 shows that the RAMO involved in the HiPIP couple (A2α in Figure 5) is very different in nature from the RAMO involved in the ferredoxin couple (B2α in Figure 5). The RAMO of HiPIP is the HOMO of the $[Fe_4S_4]^{2+}$ resting form and has 50% ligand character. Removal of an electron from this orbital upon oxidation results in a limited change in electron−electron repulsion, and thus the system needs less electronic relaxation for charge compensation.

Alternatively, the redox process in the ferredoxin couple is quite different from that of the HiPIP couple. The RAMO, leading to the biologically relevant $S = 1/2$ reduced state of the ferredoxin couple is the LUMO in Figure 5, which has only 6% ligand character. Adding one electron to this RAMO, localized mainly on the metal centers, leads to a large increase in metal-centered electron−electron repulsion, and this induces electronic relaxation, redistributing the electron density onto the ligands to compensate for the excess charge.

Functional Relevance. As mentioned above, the RAMO for HiPIP and ferredoxin are different in nature. The coefficient of the ligand character in the RAMO couples the cluster into the protein superexchange pathways for ET.[38] Thus, HiPIPs with greater ligand character in the RAMO (and low electronic relaxation) will have better superexchange pathways for electron transport between the cluster and the surface of the protein. This is required in HiPIP for efficient electron transport, as this Fe_4S_4 active site is buried in the hydrophobic core of the protein (Figure 7b).[39] Also, most of the ligand character in the RAMO of HiPIP is sulfide. There is a highly conserved H-bond to the sulfide in the HiPIP proteins. From the crystal structures of oxidized and resting HiPIP from *C. vinosum*, the $[Fe_2S_2]^{+}$ subcluster containing the H-bond to the sulfide is the redox-active subcluster.[40] Thus, this H-bond may provide an ET pathway into the cluster.

Alternatively, the active site of ferredoxin is at the surface of the protein and is solvent-exposed (Figure 7a).[41] This correlates with the fact that the RAMO has very little ligand character (6%) (and significant electronic relaxation) and, hence, only a limited coupling into the protein superexchange pathways. Thus, efficient ET requires a direct interaction with the redox partner as would be the case for the solvent-exposed cofactor of the four-iron ferredoxin.

Acknowledgment. This research was supported by NSF CHE-9980549 (E.I.S.), NIH RR-01209 (K.O.H.), NIH GM 28856 (R.H.H.), and NSERC Operating Grant 171359 (L.D.E.). Stanford Synchrotron Radiation Laboratory operations are funded by the Department of Energy, Office of Basic Energy Sciences. The SSRL Structural Molecular Biology Program is supported by the National Institutes of Health, National Center for Research Resources, Biomedical Technology Program, and by the Department of Energy, Office of Biological and Environmental Research. A.D. acknowledges Dr. P. Frank and Dr. A. J. Skulan for helpful discussions.

Supporting Information Available: The expanded energy region plots of the data, the C_2 symmetric *x*,*y*,*z* coordinates used for calculation, a sample input file used for ADF, and the individual DOS of sulfide and thiolate. This material is available free of charge via the Internet at http://pubs.acs.org.

JA0484956

(38) (a) Kennepohl, P.; Solomon, E. I. *Inorg. Chem.* **2003**, *42*, 696. (b) Lowery, M. D.; Guckert, J. A.; Gebhard, M. S.; Solomon, E. I. *J. Am. Chem. Soc.* **1993**, *115*, 3012. (c) Liang, C. X.; Newton, M. D. *J. Phys. Chem.* **1992**, *96*, 2855.
(39) Heering H. A.; Bulsink Y. B. M.; Hagen W. R.; Meyer T. E. *Biochemistry* **1995**, *34*, 14675.
(40) (a) Bertini, I.; Dikiy, A.; Kastrau, D. H.; Luchinat, C.; Sompornpisut, P. *Biochemistry* **1995**, *34*, 9851. (b) Carter, C. W., Jr.; Kraut, J.; Freer, S. T.; Xuong, N.-H.; Alden, R. A.; Bartsch, R. G. *J. Biol. Chem.* **1974**, *249*, 4212.
(41) Fukuyama, K.; Okada, T.; Kakuta, Y.; Takahashi, Y. *J. Mol. Biol.* **2002**, *315*, 1155.